

# Interpretable Motion Planner for Urban Driving via Hierarchical Imitation Learning

Bikun Wang, Zhipeng Wang, Chenhao Zhu, Zhiqiang Zhang, Zhichen Wang, Penghong Lin, Jingchu Liu and Qian Zhang.

Horizon Robotics

**Abstract**—Learning-based approaches have achieved impressive performance for autonomous driving and an increasing number of data-driven works are being studied in the decision-making and planning module. However, the reliability and the stability of the neural network is still full of challenges. In this paper, we introduce a hierarchical imitation method including a high-level grid-based behavior planner and a low-level trajectory planner, which is not only an individual data-driven driving policy and can also be easily embedded into the rule-based architecture. We evaluate our method both in closed-loop simulation and real world driving, and demonstrate the neural network planner has outstanding performance in complex urban autonomous driving scenarios.

## I. INTRODUCTION

Autonomous driving in complex urban environments is full of challenges, especially the motion planning module in modern autonomy stacks. The mainstream decision-making and motion planning solution remain traditional rule-based or optimization-based methods, which are difficult to handle with the large number of driving rules and computing resources. Learning-based methods develop fast and imitation learning approaches seem the most likely promising way to solve the bottleneck in decision-making and motion planning modules in the short-term.

The main idea of imitation learning is to learn either a cost function or a direct policy using expert demonstrations, and these supervised learning approaches such as behavior cloning have become popular due to a stable and controllable training process. Large amounts of human driving data will be the natural experts' demonstrations in autonomous driving task and the DAgger methods further enhance the diversity of data, which both make imitation learning related work rapidly grow in autonomous driving.

However, most imitation learning works in AD tasks only focus on the motion planning part with a specific route or a pixel-level goal due to complex state-action space and plenty of sensor signals making the task difficult to learn. In practice, generating a lane-level route or a pixel-level goal is also a challenging and costly problem. Moreover, another challenge of the learning-based method is using the neural network as a black box lack of security and interpretability, especially end-to-end learning studies.

In this paper, we propose VTT, a high-level value path planner and a low-level executable trajectory planner based on transformer architecture. Integrating decision-making and

motion planning as a unified architecture, VTT generates an executable long time horizon trajectory with bird's-eye view (BEV) representation and goal candidates like a real human driver. The BEV inputs include other dynamic agents' occupancy and static road map rasterization which can either be perception output by camera or a high-definition map (HD-map). Maneuver waypoints or goal candidates from navigation system provide low-definition regions for ego vehicles as a condition input. Both inputs are in the rasterized format as in Fig1. Therefore, the planner will generate a reference route conditioned on the goal regions and also a trajectory conditioned on the preferred route path for the controller.

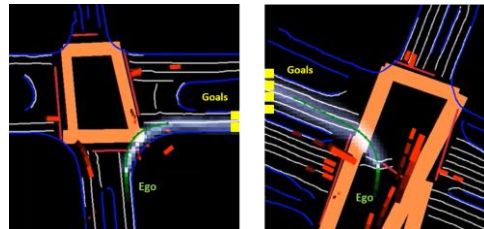


Fig1. Input and output representation of the system

Summarize the main contributions of this paper:

- A novel hierarchical transformer-based imitation learning architecture that learns a safe high-level path-selection policy and a low-level trajectory generator policy with simple low-definition arbitrary goal candidates and BEV information which is easy to use camera perception results rather than HD-map.
- Jointly generating both executable trajectory and cost map, our model is highly interpretable and convenient for rule-based intervention, which makes the system more secure and controllable.
- We demonstrate the effectiveness of our approach in real-world driving in the urban environment of downtown.

## II. RELATED WORK

**Imitation learning** is widely used in robotics and machine learning literature, and there are more and more research applied in autonomous driving. The main stream of the method is learning a direct trajectory or low-level control variable [4][17][24][26][29][30][38], and most of the works use BEV as the inputs. Some other works learning a pixel-

wise level cost function rather than a direct trajectory [19][22][41]. Besides, there are some end-to-end research using raw 6V pictures rather than BEV inputs [34][42], which is more challenging due to input feature representation learning. Considering interpretability and practicability, our work focuses on mid-to-mid tasks with BEV inputs and generates both trajectory and cost maps.

**Reinforcement learning** is a potential application in autonomous driving to optimize the imitation model with proper reward design. It will alleviate the imitation data shift phenomenon and leverage the model learning out of data distribution. Combining imitation learning and reinforcement learning is trend in autonomous driving studies [43][44][45].

**Trajectory Forecasting** Both focus on the executable vehicle trajectory, trajectory forecasting task using deep learning method develop more rapidly [5][6][8][9][10][11][12][13][14][15][16]. Some works predict the agents' trajectory in a planning way. P2T learns trajectory distribution using the IRL method [5], but the method cannot be trained end to end. [16] presents an end-to-end method using the VIN and sampling method. Jointly learning trajectory both from agents and ego, prediction and planning tasks are getting closer, and our work is inspired by these method, especially P2T as in [5]. We will introduce the comparison between our work and the original P2T work in the section afterwards.

**Transformer** obtain impressive results in many research areas including imitation learning and reinforcement learning. The transformer has better encoding ability than CNN and some transformer-based planning tasks get outstanding performance [46][47][48]. Our work is also based on transformer encoder and the architecture has proved better performance in the section below.

### III. BACKGROUND

#### A. Markov Decision Process

The problem of path planning in autonomous driving can be simplified to the occupancy grid planning problem based on a Markov Decision Process,  $\mathcal{M} = \{S, \mathcal{A}, \mathcal{T}, r, \gamma\}$  with a time horizon N. The state S represents the spatial 2-D cells space on the BEV field of view. The action space is grid moving actions function in adjacent grids including {up, down, left, right, up-left, up-right, down-left, down-right, end}. With a deterministic transition function  $\mathcal{T}$ , r is the reward and  $\gamma$  is the discount. Given the goal and initial state, the learning policy  $\pi$  is designed to find the maximum value which is the expected discounted sum of rewards over a fixed time horizon as in formula (1).

$$V^\pi(s) = \mathbb{E}^\pi \left[ \sum_{t=0}^T \gamma^t r(s_t, a_t) \right] \quad (1)$$

#### B. Value Iteration Network

Since the convolutional neural networks using kernels traverse the spatial feature, the MDP can be expressed as convolutional calculations as in [1]. Using deterministic transition as the convolutional 3x3 kernel weights, the expected value is calculated iteratively from the goal state to the start state as an approximation of dynamic programming.

Also, the spatial reward map will be learned from expert demonstrations. The VIN block utilizes a fully differentiable network to solve the grid path finding problem with stable training process and we leverage the VIN block in our model to learn a route as described in section below.

### IV. METHODOLOGY

In this section we describe VTT including input representation, high-level route selection policy based on MDP and low-level continuous trajectory policy. The whole picture of the model is shown as in Fig.2. Finally, we describe the loss design and the training strategy.

#### A. Model Architecture

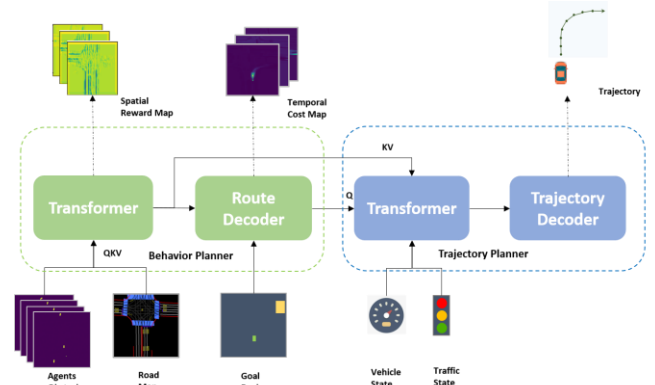


Fig2. Model architecture of the value trajectory transformer

The mid to mid imitation model VTT contains a behavior planner and trajectory planner and the planners have different inputs and outputs.

*Input representation:*

- Road map: ego-centric BEV map in which the self-driving vehicle (SDV) is always at a fixed location containing basic elements of the driving road. This input can either come from perception results based on raw camera input or HD-map.
- Agents: same BEV as road map containing the current and past dynamic obstacles occupancy on multiple channel binary images.
- Goal Regions: achieved from navigation system, the goal regions are low-definition pixel blocks on a binary image which indicate the probable driving direction on the road map. Without lane-level recommendation, VTT learns jointly the route and the trajectory.
- Dynamic states: traffic lights state and SDV speed.

*Output representation:*

- Reward/cost map: Indicating the spatial and temporal expert demonstration probability, a static reward map and multi-channel cost map will be generated as middle output. Implicitly representing the model interpretability, the pixel-level map information also can influence a rule-based planner to keep the safety of the whole system.
- Trajectory: a long time horizon trajectory is generated in 6 seconds with a 2Hz sampling frequency. The number of waypoints is the same as the dynamic cost

map channels.

### B. High-level Behavior Planner

In the high-level module, the VIN block is used for generating the spatial value map by calculating the reward map iteratively as in Fig3. First, the reward map and the image feature are generated from the upper transformer encoding block with the BEV inputs. With strong spatial modeling ability, the cross-attention mechanism learns the reward function better than CNN architecture. In order to calculate the MDP state transition, the reward map from the transformer encoding and the goal map will be involved in the convolution calculation in a 3x3 kernel. Secondly, with the approximate value iteration, we can get a goal conditioned grid transition policy which is non-stationary at different time horizon k. The value iteration process is defined as in formula (2).

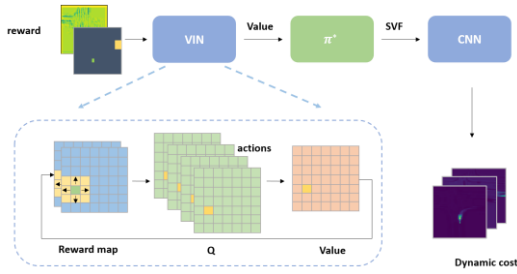


Fig3. Simple schematic diagram of the high-level route decoder

$$\begin{aligned}
 Q^k(s, a) &= r_\theta(s) + V^k(s')s' = T(s, a) \\
 V^{k-1}(s) &= \log \sum_a \exp^{Q^k(s, a)} \\
 \pi_\theta^k &= \exp^{Q^k(s, a) - V^k(s)}
 \end{aligned} \quad (2)$$

With policy propagation, the route path probability in the grid map can be generated by calculating state visit frequency (SVF) step by step. Starting in the initial ego state, the states distribution in K steps is represented in K steps SVFs which are spatially related by single step grid transition as in formula (3). And then we add some basic CNN layers to make the SVFs into temporal cost maps and the channel of the cost maps is same as the final trajectory horizon correspondingly. Given approximate location of future ego planning waypoints, these cost maps are not interpretable midline output and also the query of the low-level planner transformer encoding input.

$$Svf^{k+1}(s') = \sum_{s, a} \pi_\theta^k(a|s) Svf^k(s) \quad (3)$$

### C. Low-level Trajectory Planner

Considering cost attention as query of the low-level transformer input, the other input key-value are from the high-level transformer output feature embedding fusing dynamic states input. In the low-level module, we employ a RNN head to generate the future waypoints. The LSTM encoder produces direct control signal acceleration and curvature and a simple bicycle model will calculate the corresponding specific location.

$$h_k = LSTM_\theta(h_{k-1}, x_{k-1}) \quad (4)$$

The trajectory head is as in Fig4 and the RNN architecture will make the adjacent waypoints temporal related to each other and the kinetic model as in formula (5) will make the trajectory more controllable. Considering the control action outputs as waypoints delta incensement, we can easily apply the control constraints to make the trajectory more executable.

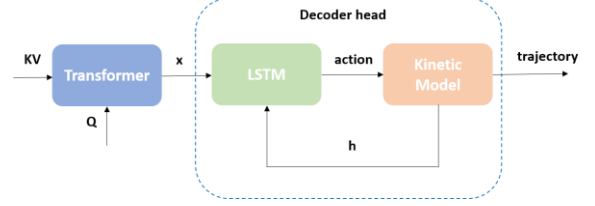


Fig4. RNN-based trajectory head

$$\begin{cases}
 x_{t+1} = x_t + v_t \cos(\theta_t) \Delta t \\
 y_{t+1} = y_t + v_t \sin(\theta_t) \Delta t \\
 \theta_{t+1} = \theta_t + v_t \kappa_t \Delta t \\
 v_{t+1} = v_t + a_t \Delta t
 \end{cases} \quad \kappa_t \approx \frac{\tan(\delta_t)}{L} \quad (5)$$

### D. Loss Design

Both the high-level and the low-level policy are supervised by expert demonstrations, which is also known as behavior cloning (BC). The total loss consists of four main components as below, including high planner loss, low planner loss, cost loss and auxiliary loss, and  $\lambda$  is a tunable parameter.

$$\mathcal{L} = \lambda_h \mathcal{L}_{high} + \lambda_l \mathcal{L}_{low} + \lambda_c \mathcal{L}_{cost} + \lambda_a \mathcal{L}_{aux} \quad (6)$$

The high loss is the normal BC loss, to reduce the distribution gap of the learning weights and the experts as in formula (7). We use L1 loss to mimic the experts' trajectories and the output states contain the waypoint coordinates, yaw angle and ego speed as defined  $s_t = \{x_t, y_t, \theta_t, v_t\}$ . Besides, as the trajectory is generated from the kinetic model, a L2 regularization penalty is applied to the network output to keep the smoothness of the trajectory, which is actually constraint of the acceleration and the curvature as in formula (8).

$$\mathcal{L}_{high} = \mathbb{E}_{s, a \in \pi_\theta} \log \pi_\theta(a|s) \quad (7)$$

$$\mathcal{L}_{low} = \sum_{t=1}^K \|s_t - s_t^{gt}\|_1 + \alpha \|a_t\|_2 + \beta \|\kappa_t\|_2 \quad (8)$$

With the policy propagation from the behavior planner, we can get the grid-based state visit frequency in the form of the heat-map. We encode the SVFs into the dynamic costs which represent the probability distribution in a specific time step, and the costs are supervised using pixel-wise focal loss as  $\mathcal{H}$ . The time horizon is same as the trajectory output. The ground truth of the cost map is the expert occupancy grid in different time steps.

$$\mathcal{L}_{cost} = \sum_{t=1}^K \mathcal{H}(C_t(x, y), C_t^{gt}(x, y)) \quad (9)$$

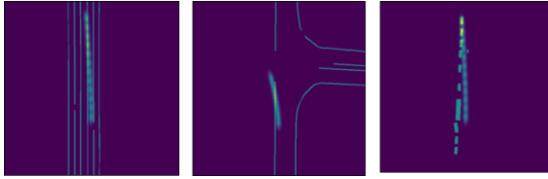


Fig4. Differentiable rasterized auxiliary loss

In order to decrease the occurrence of dangerous behaviors, we calculate potential off-road and collision probability using the rasterized trajectory mask with the environment mask, which is the auxiliary loss same as in [20][24]. Every trajectory waypoint  $s_t$  is rasterized into an occupancy grid through ellipse Gaussian kernels with the vehicle length and width, where  $\mathcal{G}(s_t) = \mathcal{N}(\mu \Sigma)$  is the rasterization function to convert trajectory into the vehicle box-like shape occupancy as in Fig4.  $\mathcal{T}_i^{raster}$  is the given binary masks including the static road topology and dynamic obstacles. The calculation of the rasterized auxiliary loss is defined in formula (10).

$$\mathcal{L}_{aux} = \sum_{t=1}^K \sum_{i=1}^N \mathcal{G}(s_t) \mathcal{T}_i^{raster} \quad (10)$$

#### E. Data Augmentation

Proper data augmentation will make policy learning from the data out of the experts demonstration distribution. We disturb the initial start waypoint of the trajectory with a random displacement and heading angle similar to [4]. Then update the BEV inputs with the perturbation error correspondingly. Since the perturbation start point and the fixed endpoint is known, we use a lightweight optimizer to calculate the new trajectory ground truth with motion constraints which keep the new trajectory is the feasible action to recover from the perturbation error.

Since the DAgger methods help alleviate the data distribution shift problem, we train the network in a close-loop way. After every training epoch, the performance of the current learned policy in the experts datasets will generate new synthesized data samples with the calibrated trajectory ground truth which is also generated by the optimizer as mentioned above. The key difference from the perturbation method is the noise coming from the outside randomly or current policy itself.

## V. EXPERIMENTS

### A. open-loop evaluation

We evaluate our method on real-world driving datasets collected in the urban environment called TDT datasets. A variety of urban driving scenarios data was collected including multi-lanes and intersections for more than 50 hours. Our BEV inputs filed with view including the road map and the 2s dynamic agents occupancy rasterization are 102.4m x 102.4m with 0.2m/pixel resolution, which is 512x512 corresponding to the image size. The position of the ego car is fixed at (362, 256) of the image with 72.4m in front and 30m in back and both 51.2m to the left and right. The output trajectory is 2Hz

with total 6s planning horizon, and the time step between every adjacent waypoint is 0.5s. Although the history information of the ego vehicle will improve the open-loop results especially the expert similarity, we do not use any history information which will lead to causal confusion as mentioned in [3]. The detail configuration parameter is as in table below.

TABLE I. MODEL CONFIGURATION PARAMETERS

<i>configuration parameters</i>	<i>value</i>
Inputs images size	512, 512
Inputs Pixel resolution	0.2m/pixel
History agents information	2s
Value iteration horizon	50
Number of grid actions	9
Cost map images size	65, 65
Cost map pixel resolution	1.6m/pixel
Trajectory horizon	6s
Number of cost maps	12
Number of waypoints	12
Learning rate	1e-4

The open-loop evaluation mainly reveals the learning ability of the model that approaches the experts' distribution and also obeys the potential obvious constraints. svf\_diff is the difference between the predicted path from high-level policy propagation and the expert binary distribution. We use L2 distance between the learning trajectory and the expert trajectory to represent the expert similarity, which is also known as ADE(average displacement error). Also, we calculate the future ego occupancy along with the predicted trajectory to check the intersection with the future obstacles and the road edge to represent the potential crash rate and the off-road rate. Every way point is calculated separately in the specific time horizon.

TABLE II. OPENLOOP TEST RESULTS

baseline	SVF Diff (%)	ADE(m)		Crash rate (%)		Off-Road rate (%)	
		average	final	average	final	average	final
P2T	0.80	1.48	3.58	0.71	1.80	0.12	0.2
VTN	0.85	1.47	3.56	0.70	1.72	0.09	0.22
<b>VTT</b>	<b>0.73</b>	<b>1.40</b>	<b>3,35</b>	<b>0.63</b>	<b>1.68</b>	<b>0.05</b>	<b>0.22</b>

From the table, the proposed approach VTT achieves the best performance from all sides. The P2T baseline is our first baseline using the method [5] containing a reward model and a trajectory generator. However inputs of the low-level policy are sampled and cropped ROI features by the high-level policy instead of learning costs, which is cannot trained end to end. We implement the P2T method in the TDT datasets using the open source code The VTN baseline is the same as VTT with only CNN encoding rather than transformer.

Interpretability is very significant in the driving system and it will not only help explain neural network learned distribution but also benefit to the rule-based planning system. Our learning cost volume represents the occurrence heat-map distribution at a specific time step as in fig5. The white area in the left picture is the learned route path and the yellow trajectory is the learned trajectory as the green is the ground truth. As being spatial attention, these costs indicate the most likely position where the experts will pass. The middle outputs can not only help with bad case explanation study, but are also convenient to add rule-based manual intervention as the goal-keeper of the whole system.

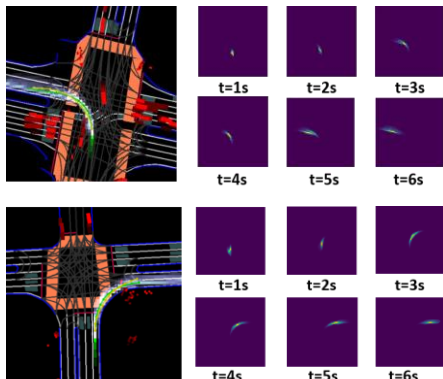


Fig5 visualization of representative scenarios planning outputs with different time horizon learning costs

### B. close-loop evaluation

Generally, we employ two types of closed-loop simulations, world-sim and log-sim respectively. In the world-sim, scenarios including static and dynamic elements are generated manually, whereas scene information in the log-sim are extracted from field tests and replayed with minor modification in the simulation. In this study, log-sim is taken as the major approach to testing and evaluation under consideration that field test data provides us with more real and complex scenarios. Log data used in the simulation are clipped from field tests with expert trajectories, in which each lasts tens of seconds and various scenarios are covered, such as following, right turn, left turn, U-turn, lane changing etc.

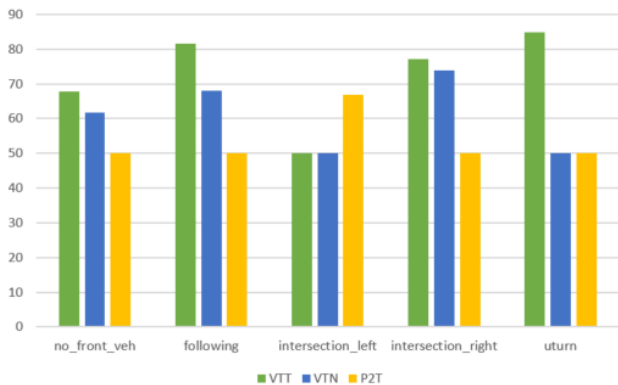


Fig6 close-loop simulation results with typical scenarios

Same as the open-loop evaluation comparison, the closed-loop simulation performance which compares the VTT model, VTN model and P2T model are shown as follows. Five scenarios are considered, including cruising without front vehicles, following, left turn, right turn and u turn. From the results, we can see that the VTT model achieve better performance in most driving test scenarios. The vertical axis represent the total simulation score considering the scenario completeness, expert similarity and comfort. The detailed calculation metric is described in appendix.

### C. Real-World Driving

We implement our approach in the real world with Horizon Journey 5 chips as integrated hardware. Our model is quantized into an int8 format with less accuracy loss and achieves 80~100FPS inference speed. Instead of using large amounts of data, we only train our model in our small datasets mentioned before including 50h+ human driving data to validate the model performance. The raw trajectory output from the network is directly translated to control signal through a MPC controller with barely rule constraints. The self-driving system is tested in the downtown environment under the supervision of human safety drivers. Our approach demonstrates positive human-like driving ability facing all kinds of urban driving challenges, including lane-keeping, lane-changing, turning left/right at intersection and U-turn. Especially in the right turning scenario, the network trajectory is more comfortable with a lower curvature than the reference drive line, which acts more like a real human driver.

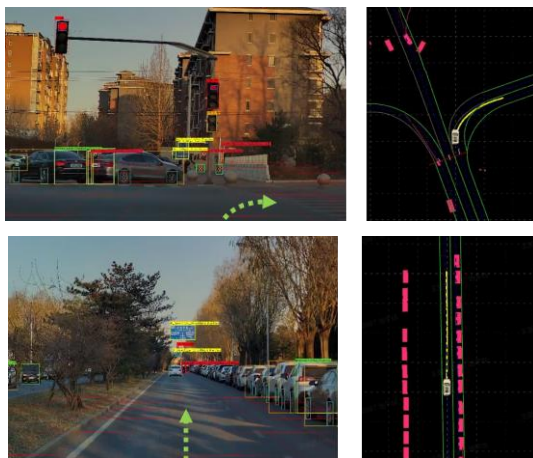


Fig7 example of real world testing scenario

## VI. CONCLUSION

We proposed an explainable hierarchical neural network motion planner using imitation learning for urban autonomous driving applications. Integrating decision-making and motion planning, the high-level policy decodes the goal regions into coarse route occupancy and the low-level policy generates waypoint trajectory. The hierarchical architecture not only provides middle interpretable cost outputs, but also guarantees stable training convergence. We demonstrate our model performance both in simulation and real-world driving and our approach achieves outstanding performance in complex urban driving scenarios. In the future, we will continue to explore the limits of imitation learning by enlarging expert data and

focusing on improving generalization performance in extremely challenging driving scenarios. Besides, reinforcement learning is also another way to improve model performance in interaction with static and dynamic agents.

## REFERENCES

- [1] Tamar, A., Wu, Y., Thomas, G., Levine, S. & Abbeel, P. Value Iteration Networks. In *NeurIPS*, 2016, pp. 2154-2162.
- [2] S. Ross, G. J. Gordon, and J. A. Bagnell, "A Reduction of Imitation Learning and Structured Prediction to No-Regret Online Learning," in *AISTATS*, 2011, pp. 627–635.
- [3] P. de Haan, D. Jayaraman, and S. Levine, "Causal Confusion in Imitation Learning," in *NeurIPS*, 2019.
- [4] M. Bansal, A. Krizhevsky, and A. Ogale, "ChauffeurNet: Learning to Drive by Imitating the Best and Synthesizing the Worst," in *RSS*, 2019.
- [5] N. Deo and M. M. Trivedi, "Trajectory Forecasts in Unknown Environments Conditioned on Grid-Based Plans," in *CVPR*, 2021.
- [6] N. Nayakanti, R. Al-Rfou, A. Zhou, K. Goel, K. S. Refaat, and B. Sapp, "Wayformer: Motion Forecasting via Simple & Efficient Attention Networks." in *CVPR*, 2022.
- [7] M. Wulfmeier, P. Ondruska, and I. Posner, "Maximum Entropy Deep Inverse Reinforcement Learning," arXiv preprint arXiv:1507.04888, 2015.
- [8] H. Zhao et al., "TNT: Target-driveN Trajectory Prediction," In *Conference on Robot Learning*, 2020.
- [9] T. Phan-Minh, E. C. Grigore, F. A. Boulton, O. Beijbom, and E. M. Wolff, "CoverNet: Multimodal Behavior Prediction using Trajectory Sets," In *CVPR*, pages 14074–14083, 2020.
- [10] Y. Chai, B. Sapp, M. Bansal, and D. Anguelov, "MultiPath: Multiple Probabilistic Anchor Trajectory Hypotheses for Behavior Prediction," in *Conference on Robot Learning*. PMLR, 2020, pp. 86–99.
- [11] A. Cui, S. Casas, A. Sadat, R. Liao, and R. Urtasun, "LookOut: Diverse Multi-Future Prediction and Planning for Self-Driving," in *ICCV*, 2021.
- [12] A. Hu et al., "FIERY: Future Instance Prediction in Bird's-Eye View from Surround Monocular Cameras." in *ICCV*, 2021.
- [13] A. Kamenev et al., "PredictionNet: Real-Time Joint Probabilistic Traffic Prediction for Planning, Control, and Simulation," in *ICRA*, 2022.
- [14] T. Gilles, S. Sabatini, D. Tsishkou, B. Stanculescu, and F. Moutarde, "HOME: Heatmap Output for future Motion Estimation," in *ITSC*, 2021.
- [15] K. Guo, W. Liu, and J. Pan, "End-to-End Trajectory Distribution Prediction Based on Occupancy Grid Maps." in *CVPR*, 2022.
- [16] L. F. Chiara, P. Coscia, S. Das, S. Calderara, R. Cucchiara, and L. Ballan, "Goal-driven Self-Attentive Recurrent Networks for Trajectory Prediction," in *CVPR*, 2022.
- [17] J. Chen, B. Yuan, and M. Tomizuka, "Deep Imitation Learning for Autonomous Driving in Generic Urban Scenarios with Enhanced Safety," in *IROS*, 2019.
- [18] J. Liu, W. Zeng, R. Urtasun, and E. Yumer, "Deep Structured Reactive Planning," in *ICRA*, 2021.
- [19] W. Zeng, S. Wang, R. Liao, Y. Chen, B. Yang, and R. Urtasun, "DSDNet: Deep Structured self-Driving Network," ArXiv200806041 Cs, Aug. 2020, Accessed: Dec. 26, 2021.
- [20] H. Cui, H. Shajari, S. Yalamanchi, and N. Djuric, "Ellipse Loss for Scene-Compliant Motion Prediction," in *ICRA*, 2021.
- [21] N. Baram, O. Anschel, I. Caspi, and S. Mannor, "End-to-End Differentiable Adversarial Imitation Learning," in *ICML*, 2017.
- [22] W. Zeng et al., "End-to-end Interpretable Neural Motion Planner," in *CVPR*, 2019.
- [23] A. Prakash, A. Behl, E. Ohn-Bar, K. Chitta, and A. Geiger, "Exploring Data Aggregation in Policy Learning for Vision-Based Urban Autonomous Driving," in *CVPR*, 2020, pp. 11760–11770.
- [24] J. Zhou et al., "Exploring Imitation Learning for Autonomous Driving with Feedback Synthesizer and Differentiable Rasterization," in *IROS*, 2021.
- [25] F. Codevilla, E. Santana, A. Lopez, and A. Gaidon, "Exploring the Limitations of Behavior Cloning for Autonomous Driving," in *ICCV*, 2019, pp. 9328–9337.
- [26] E. Bronstein et al., "Hierarchical Model-Based Imitation Learning for Planning in Autonomous Driving." in *IROS*, 2022.
- [27] Y. Wang, D. Zhang, J. Wang, Z. Chen, Y. Wang, and R. Xiong, "Imitation Learning of Hierarchical Driving Model: from Continuous Intention to Continuous Trajectory," *IEEE Robotics and Automation Letters*, 2020.
- [28] A. Sadat, M. Ren, A. Pokrovsky, Y.-C. Lin, E. Yumer, and R. Urtasun, "Jointly Learnable Behavior and Trajectory Planning for Self-Driving Vehicles," in *IROS*, 2019.
- [29] [D. Chen, B. Zhou, V. Koltun, and P. Krähenbühl, "Learning by Cheating," ArXiv191212294 Cs, Dec. 2019.
- [30] D. Chen and P. Krähenbühl, "Learning from All Vehicles," in *CVPR*, 2022.
- [31] J. Wang, Y. Wang, D. Zhang, Y. Yang, and R. Xiong, "Learning hierarchical behavior and motion planning for autonomous driving." in *IROS*, 2022.
- [32] H. Wang, P. Cai, Y. Sun, L. Wang, and M. Liu, "Learning Interpretable End-to-End Vision-Based Motion Planning for Autonomous Driving with Optical Flow Distillation," in *ICRA*, 2021, Accessed: Sep. 17, 2021.
- [33] H. Song, D. Luan, W. Ding, M. Y. Wang, and Q. Chen, "Learning to Predict Vehicle Trajectories with Model-based Planning," in *Conference on Robot Learning*, 2021.
- [34] S. Casas, A. Sadat, and R. Urtasun, "MP3: A Unified Model to Map, Perceive, Predict and Plan," in *CVPR*, 2021, pp. 14398–14407.
- [35] H. Pulver, F. Eiras, L. Carozza, M. Hawasly, S. V. Albrecht, and S. Ramamoorthy, "PILOT: Efficient Planning by Imitation Learning and Optimisation for Safe Autonomous Driving," in *IROS*, 2021.
- [36] M. Vitelli et al., "SafetyNet: Safe planning for real-world self-driving vehicles using machine-learned policies," in *ICRA*, 2022.
- [37] A. Jamgochian, E. Buehler, J. Fischer, and M. J. Kochenderfer, "SHAIL: Safety-Aware Hierarchical Adversarial Imitation Learning for Autonomous Driving in Urban Environments." arXiv, Apr. 04, 2022.
- [38] P. Wu, X. Jia, L. Chen, J. Yan, H. Li, and Y. Qiao, "Trajectory-guided Control Prediction for End-to-end Autonomous Driving: A Simple yet Strong Baseline." in *NeurIPS*, 2022.
- [39] [O. Scheel, L. Bergamini, M. Wolczyk, B. Osiński, and P. Ondruska, "Urban Driver: Learning to Drive from Real-world Demonstrations Using Policy Gradients," In *Conference on Robot Learning*, 2021.
- [40] J. Hawke et al., "Urban Driving with Conditional Imitation Learning," in *ICRA*, 2021.
- [41] M. Wulfmeier, D. Z. Wang, and I. Posner, "Watch This: Scalable Cost-Function Learning for Path Planning in Urban Environments," in *IROS*, 2016. [Online]. Available: <http://arxiv.org/abs/1607.02329>
- [42] Shengchao. Hu et al., "ST-P3: End-to-end Vision-based Autonomous Driving via Spatial-Temporal Feature Learning," in *ECCV*, 2022.
- [43] Y. Lu et al., "Imitation Is Not Enough: Robustifying Imitation with Reinforcement Learning for Challenging Driving Scenarios." arXiv, Dec. 21, 2022. Accessed: Feb. 03, 2023.
- [44] F. Gao et al., "ApolloRL: a Reinforcement Learning Platform for Autonomous Driving," ArXiv220112609 Cs Stat, Jan. 2022, Accessed: Mar. 11, 2022.
- [45] Z. Zhang, A. Liniger, D. Dai, F. Yu, and L. Van Gool, "End-to-End Urban Driving by Imitating a Reinforcement Learning Coach," in *ICCV*, 2021.
- [46] K. Renz, K. Chitta, O.-B. Mercea, A. S. Koepke, Z. Akata, and A. Geiger, "PlanT: Explainable Planning Transformers via Object-Level Representations." In *Conference on Robot Learning*, 2022.
- [47] L. Chen et al., "Decision Transformer: Reinforcement Learning via Sequence Modeling,"
- [48] M. Janner, Q. Li, and S. Levine, "Reinforcement Learning as One Big Sequence Modeling Problem," in *NeurIPS*, 2021.

## Appendix A

### Close-loop evaluation metric

To leverage the availability of expert data in the log-sim, metrics are designed to:

- evaluate both scenario-specific and overall performance of our motion planner with comparison to expert data and other planners
- quantify the similarity between trajectories as well as paths generated by our motion planner and expert trajectories

Major evaluation metrics are route completion degree, path and trajectory similarity and overall performance.

- Route completion degree

$$RC = \frac{s_{sim}}{s_{expert}} \quad (11)$$

- $s_{sim}$ : travel distance of ego in the logsim without collision or violating regulations
- $s_{expert}$ : travel distance of the expert

- Path similarity

$$S_{path} = \min\left(OWD(\tau_{sim}, \tau_{expert}), OWD(\tau_{expert}, \tau_{sim})\right) \quad (12)$$

- $S_{path}$ : similarity of simulated ego path compared to expert path
- $\tau_{sim}$ : ego path
- $\tau_{expert}$ : expert path
- $OWD$ : one-way distance method to evaluate the similarity between two paths

- Trajectory similarity

$$S_{traj} = LSED(\tau_{sim}, \tau_{expert}) \quad (13)$$

- $S_{traj}$ : similarity of simulated ego trajectory compared to expert trajectory
- $\tau_{traj}$ : ego trajectory
- $\tau_{traj}$ : expert trajectory
- $LSED$ : lock-step euclidean distance method to evaluate the similarity between two trajectories

- Overall Performance

$$Score = 1/N \sum_{i=1}^N RC_i P_i \quad (14)$$

$$P_i = \prod_{j=1}^n \lambda_j^{k_{i,j}} \quad (15)$$

*Score*: overall performance of the planner in certain scenarios

- $N$ : number of simulations
- $RC_i$ : route completion degree of the  $i$  th simulation
- $P_i$ : infraction discount of the  $i$  th simulation
- $n$ : total number of infraction types which include off road, speeding, running red lights and crossing solid lines
- $\lambda_j$ : discount coefficient of infraction type  $j$
- $k_{i,j}$ : counts of infraction type  $j$  in the  $i$  th simulation